Title

INTERACTIONS OP 1.6l BeV/c ANTIPROTONS IN HYDROGEN INVOLVING TWO OUTGOING CHARGED PARTICLES

Authors

Lynch, Gerald. R.
Foulks, Robert E.
Kalbfleisch, George R.
et al.

Publication Date

1963-01-17

UCRL-10632

University of California

Ernest O. Lawrence Radiation Laboratory

INTERACTIONS OF 1.61-BeV/c ANTIPROTONS IN HYDROGEN INVOLVING TWO OUTGOING CHARGED PARTICLES

Berkeley, California

DISCLAIMER

Submitted for pub. in Phys. Rev.

UCRL-10632

UNIVERSITY OF CALIFORNIA

Lawrence Radiation Laboratory
Berkeley, California

Contract No. W-7405-eng-48

INTERACTIONS OF 1.61-BeV/c ANTIPROTONS IN HYDROGEN INVOLVING TWO OUTGOING CHARGED PARTICLES

Gerald R. Lynch, Robert E. Foulks, George R. Kalbfleisch, Sylvia Limentani, Janice B. Shafer, M. Lynn Stevenson, and Nguyen-huu Xuong

January 17, 1963

Interactions of 1.61-BeV/c Antiprotons in Hydrogen Involving Two Outgoing Charged Particles

Gerald R. Lynch, Robert E. Foulks, George R. Kalbfleisch, Sylvia Limentani, Janice B. Shafer, M. Lynn Stevenson, and Nguyen-huu Xuong

Lawrence Radiation Laboratory
University of California
Berkeley, California

January 17, 1963

ABSTRACT

Interactions of 1.61-BeV/c antiprotons in hydrogen yielding two charged particles have been studied, with particular attention to elastic scattering, single pion production, and annihilation into three or more pions. Effects of misinterpretation of events are estimated by Monte Carlo calculations. Nine partial cross sections have been measured. The elastic-scattering data show a secondary diffraction peak at about 82° in the center of mass. Single pion production is found to be consistent with charge-conjugation invariance. In the single pion events ($\bar{p} + p \rightarrow \bar{N} + N + \pi$) the predominance of low-momentum transfer exceeds that predicted by the single pion exchange formula of Chew and Low. No two-pion resonances have been observed anywhere in the data.

Interactions of 1.61-BeV/c Antiprotons in Hydrogen Involving Two Outgoing Charged Particles*

Gerald R. Lynch, Robert E. Foulks, George R. Kalbfleisch, Sylvia Limentani, Janice B. Shafer, M. Lynn Stevenson, and Nguyen-huu Xuong

Lawrence Radiation Laboratory
University of California
Berkeley, California

January 17, 1963

I. INTRODUCTION

This is a study of events with two outgoing charged particles (two prongs) among 1.61-BeV/c antiproton interactions, including elastic scatterings, annihilations, and other inelastic interactions. The events analyzed were interactions in the 72-inch hydrogen bubble chamber. Numerous papers have been written on various interactions in this film.[1-14] The most complete description of the beam and of the experiment as a whole is presented by Button et al.[2] The annihilations into kaons have been separately studied.[8] Consequently, these events are not analyzed here other than as a contamination of the other two-prong interactions. Also, the small-angle elastic scatterings ($\cos\theta > 0.80$) have not been studied because it is difficult to separate these events from the elastic pion scatterings that are in the film, and because small-angle elastic scattering has been studied near this energy by two counter groups.[15,16] The search for two-meson annihilations was to some extent a separate project, and is reported in a separate and accompanying paper.

About one half the two-prong events measured in this experiment were annihilations involving more than one neutral particle. These events upon which one cannot make kinematic fits cannot be identified. Such unidentifiable events serve as a large reservoir of events that may contaminate the less frequently occurring two- and three-body events that we wish to analyze. Therefore, considerable effort has been made to determine the extent of this contamination. An important tool in this respect has been program FAKE,[17] a Monte Carlo program that can generate events according to a particular prescription. These events can subsequently be analyzed by the same data-analysis system that processes the real events. FAKE simulates events to resemble the output of the track-reconstruction program, complete with a simulation of the measurement errors and errors due to Coulomb scattering. Thus, by using FAKE one can observe what his data-analysis system will do with events of a known type, and how often these events are classified incorrectly. The limitation of this technique is that, in order to obtain a reliable simulation of a part of an experiment, one needs to generate the events with the correct matrix element -- -- something that at best is imperfectly known.

II. THE EXPERIMENT

The events chosen to be measured were all the two-pronged events in a specified fiducial volume in the bubble chamber and in an edited sample of the film, except for those events which were obvious small-angle elastic scatterings. (Events were classified as small-angle elastic scatterings if simple scanning-table observation showed them to be coplanar with a stopping or nearly stopping proton that made an angle of at least 57° with the beam track.) In case of doubt the event was measured. All events were measured with Franckenstein measuring projectors and were processed by the PANG and KICK analysis programs.

The 3569 measured events can be classified into the following groups:

1. Interactions produced by incident pions,
2. Elastic antiproton interactions,
3. Inelastic antiproton interactions (single-pion production),
4. Annihilations producing kaons,
5. Annihilations not producing kaons (pion annihilations).

The number of events in the first group was estimated by analyzing the events that had δ rays on the incident track.[18] In the measured sample 19. ± 4% of the events were pion interactions. We estimate that the 3569 measured events came from a sample containing 8823 ± 300 visible antiproton interactions. The dominant part of the uncertainty in this number comes from the uncertainty in the number of pion interactions. We have determined that 3 ± 1 mb of the elastic-scattering events were not observed by the scanners because the angle of scattering was too small and the proton recoil was too short. Thus the 8823 antiproton interactions correspond to 93 mb rather than to the total cross section of 96 ± 2 mb.[15]

Most of the pion interactions can be removed from the sample by requiring that the incident particle have a momentum greater than some minimum value, because most of the incident pions had momenta lower than the momenta of most of the antiprotons. Whereas in 14 ± 6% of the interacting pions the measured beam momentum at the center of the chamber was greater than 1550 MeV/c, 86. ± 3% of the antiprotons have measured momenta at least this great. Therefore, the sample of events with measured beam momenta greater than 1550 MeV/c has only a 3.6 ± 1.8% pion contamination. All the analysis to be described subsequently was made by using the 2649 events in this high-momentum sample.

Using the results of the study of the annihilations into kaons,[8] we estimate 322 ± 40 events in the sample to be annihilations producing kaons. There were 110 events observed to have associated kaon decays, leaving 212 ± 40 events with kaon decays that cannot be so identified.

The events can be placed in the following experimental categories:

A. Events with beam momenta less than 1550 MeV/c,

B. Events not in A that fit antiproton elastic scattering with $\chi^2 < 30$,

C. Events not in A or B that fit one of the inelastic three-body interactions with $\chi^2 < 5$,

D. Events not in A, B, or C that are consistent with pion annihilations,

E. Events not in A, B, C, or D.

Table I shows the number of events found in these experimental categories, as well as estimates of how they are populated by the previously mentioned groups. Category E consists of 110 events with associated K decays, 23 events that fit elastic pion scattering, 6 events identified from δ rays as pion

interactions, and 80 events with measurement errors so large that classification was useless. The arguments leading to the assignments of many of the numbers in Table I will be presented when the categories are discussed in more detail.

III. ELASTIC SCATTERING

Elastic scattering at or near the energy of this experiment has been studied at small angles before.[4,15,16] None of these data gave very useful information about the scattering for c.m. angles greater than 50°, the region outside the forward diffraction peak. Therefore, the emphasis in this study was on these large-angle scatterings. It was ascertained that the scanning criteria we used to choose the events resulted in a high efficiency for including elastic scatterings that have c.m. angles greater than 36.9° ($\cos\theta = 0.80$). There were 258 such events that fitted with $\chi^2 < 30$. The number of misinterpreted events in this sample is small, probably no more than one or two. The angular distribution of these events is shown on Fig. 1. This shows that there is a secondary peak in the angular distribution near $\cos\theta = 0.15$.

Such a second-diffraction peak is predicted by simple optical models. We attempted to fit these data with an optical model of a form suggested by Greider and Glassgold.[19] The elastic differential cross section is given by

$$\frac{d\sigma}{d\Omega}(\theta) = \left| \frac{1}{2ik} \sum_{\ell=0}^{\infty} (2\ell + 1)(\eta_\ell - 1) P_\ell (\cos\theta) \right|^2,$$

and in this model the scattering amplitude is given by

$$\eta_\ell = \begin{cases} \sqrt{1-\beta}\; e^{i\alpha(\ell)} & \text{for } 0 \leq \ell < L-\Delta \\ g(\ell)\; e^{i\alpha(\ell)} & \text{for } L-\Delta \leq \ell \leq L+\Delta, \\ 1 & \text{for } \ell > L+\Delta \end{cases}$$

where $g(\ell)$ is a monotonic decreasing function that describes the shape of the proton (or rather the shape of the proton-antiproton system). It depends upon the parameter L, which is a measure of the effective radius of the proton expressed in units of angular momentum, and the parameter Δ, which is a measure of the thickness of the "edge" of the proton. The parameter L as well as the parameter Δ may be expressed in terms of an equivalent proton radius by means of the expression $R = (L + 1/2)\,\hbar/p = 0.30(L + 1/2)$ f, where p is the c.m. momentum of the incident particle. The parameter β is the opacity of the nucleus at small values of ℓ, and α is a phase. The smooth curve on Fig. 2, illustrates these optical-model parameters. The conventional phase shift δ_ℓ is related to these parameters by $\eta = e^{2i\delta_\ell}$, and for $L - \Delta \leq \ell \leq L + \Delta$, we have $\delta_\ell = \frac{\alpha_\ell}{2} - \frac{i}{2} \ln [g(\ell)]$.

In making this analysis, both the data of this experiment and the data of the previously measured differential cross sections were used. Making the maximum-likelihood analysis involved finding the maximum of the function

$$F = \sum_{i=1}^{258} \ln\left(\frac{\sigma_i}{N_p}\right) - \sum_{j=1}^{11} \frac{(\sigma_p - \sigma_j)^2}{2(\delta\,\sigma_j)^2} - \frac{(258 - N_p)^2}{2(\delta\,N_p)^2},$$

where σ_p and σ_j are the predicted and measured differential cross sections and N_p is the predicted number of events for $\cos\theta < 0.8$. The first term in F

serves to fit the shape of the angular distribution for $\cos\theta < 0.8$, the second term treats the data for $\cos\theta > 0.8$, and the third term has to do with the number of events for $\cos\theta < 0.8$.

As a first step we did a two-parameter fit by considering complete absorption at small radii; i.e., we set $\beta = 1$ and $\alpha = 0$. Such a fit, though it reproduces the general features of the data, has a very poor likelihood because it has a zero near $\cos\theta = 0.5$, and the data in this region are not consistent with the presence of a zero. Only by making α nonzero can this model give solutions having the essential features of the data and not having a zero near $\cos\theta = 0.5$. The fit to the data obtained with a four-parameter fit is shown on Fig. 2. The best fit corresponds to the parameters $L = 3.83 \pm 0.06$, $\Delta = 2.05 \pm 0.10$; $\alpha = 11.0° \pm 1.1°$, and $\beta = 0.990^{+0.003}_{-0.007}$. The uncertainties quoted are equal to the changes in the parameters that cause F to decrease by 0.5. This fit does not represent the data well. The solution obtained with this optical model depended little upon the specific form of the function $g(\ell)$. The $g(\ell)$ used for the quoted solution was

$$g(\ell) = \begin{cases} \exp\left(1 - \beta\left\{1 - 1/2\left[(L - \Delta - \ell)/\Delta\right]^2\right\}\right)^{1/2} & \text{for } L - \Delta < \ell < L \\ \exp\left\{1 - \frac{\beta}{2}\left[(L + \Delta - \ell)/\Delta\right]^2\right\}^{1/2} & \text{for } L < \ell < L + \Delta \end{cases}$$

As a final attempt to understand the data, a fit was made leaving each complex η_ℓ as a free parameter and subtracting the term

$$\left\{\frac{1}{2k}\sum_{\ell+1}^{\ell_{max}}(2\ell+1)\left[1 - \mathrm{Re}(\eta_\ell)\right] - \sigma_T\right\}^2 \Big/ (\Delta\sigma_T)^2$$

from the function F in order to constrain the fit to satisfy the optical theorem. The total cross section was taken to be $\sigma_T \pm \Delta\sigma_T = 96 \pm 4$ mb. Although this method is far short of a complete phase-shift analysis, inasmuch as spin and isospin are not taken into account, this method does not have any approximations. The $l = 5$ terms were included, and because such solutions were satisfactory, no attempt was made to include higher waves. With such a model containing many parameters -- 12 for $l_{max} = 5$ -- there is little doubt that a good fit can be made to the data. The interest is not to see if a good fit can be made, but rather to see what one can conclude from these fits. There are many different solutions giving good fits to the data and having quite different values for some of the fitted parameters. However, all the good fits are similar in character. The angular distributions predicted by the best of these fits are shown on Fig. 1 and Fig. 2. All the good 12-parameter fits have the same features as does this one: namely, in addition to the forward peak with a height of about 60 mb/sr, there is a secondary peak with a height of about 0.30 mb/sr centered at about $\cos\theta = 0.14$ and a narrow backward peak with a height of about 0.13 mb/sr. The values found for the parameters for the four best solutions are presented in Table II. The good solutions have other things in common besides agreement on the shape of the differential cross section. Figure 3 shows a plot of the values of $1 - |\eta_l|^2$ as a function of l for the four best solutions found. This quantity is proportional to the contribution to the reaction cross section and can be thought of as the opacity of the proton as seen by the antiproton for a particular partial wave. The values of F for these four solutions do not differ from one another by more than a factor of 10. We expect that this set of solutions,

though not complete, is a representative set of the possible solutions. The opacity corresponding to $\ell = 0$ is not very well determined, but it does seem to be fairly well indicated for the other partial waves.

Also, plotted on Fig. 2 and tabulated in Table II is the result of making a six-parameter fit by constraining the imaginary part of η_ℓ (and thus the real part of the scattering amplitude) to be zero. Although the likelihood for this solution is only about 10^{-4} that of the best solutions, it certainly does not appear to be a poor solution. The opacity predictions corresponding to this fit are in good agreement with those of the good 12-parameter fits.

The integrated elastic cross sections predicted by the good fits to the data yield 31.1 ± 2.0 mb.

IV. INELASTIC SCATTERING

The reactions

$$\bar{p} + p \rightarrow \bar{p} + p + \pi^0 , \quad (1)$$

$$\bar{p} + p \rightarrow \bar{p} + n + \pi^+ , \quad (2)$$

and

$$\bar{p} + p \rightarrow \bar{n} + p + \pi^- . \quad (3)$$

are of interest because they can provide a test of charge-conjugation invariance (C) in strong interactions. The proton-antiproton initial state is an eigenstate of both CP and CR, and these invariance principles demand among other things that

(a) the cross sections for (2) and (3) be equal,

(b) the angular distributions of the $\bar{p}$ and the p in (1) be reflections of each other,

and

(c) the angular distributions of the $\bar{p}$ and the n in (2) be reflections of the angular distributions of the p and the $\bar{n}$, respectively, in (3).

If we assume the validity of the conservation of parity (P) in strong interactions or the validity of invariance under spatial rotation (R), then tests of these statements constitute tests of charge-conjugation invariance in these reactions. A more detailed statement of the predictions of charge-exchange invariance is presented by Pais[20] and by Xuong et al.[4]

The sample of events analyzed as inelastic-scattering events are those events which did not fit any two-body final state and which had a $\chi^2 < 5$ for one of the three inelastic reactions. Many events fit more than one of these reactions. For almost all of these events, ionization observations removed the ambiguities. The sample was found to contain 137 events that fitted (1), 108 that fitted (2), and 98 that fitted (3). Table III shows the estimates of the compositions of these groups of events, or how many misinterpreted events each group contains. The estimates of background events from annihilations involving kaons were made by analyzing those events having associated kaon decays. The estimates of the background events from annihilations yielding only pions were obtained by using program FAKE. The FAKE annihilation sample is described in Sec. V. These data indicate that the $\bar{p}p\pi^o$ events are about 90% pure, whereas the samples for the other two inelastic modes are only about 70% pure. The fact that these latter samples are not very pure makes the tests of charge-conjugation invariance more difficult. The cross sections obtained for these reactions are

$$\sigma_{\bar{p}p\pi^0} = 1.85 \pm 0.22 \text{ mb},$$

$$\sigma_{p\bar{n}\pi^-} = 1.19 \pm 0.16 \text{ mb},$$

and

$$\sigma_{\bar{p}n\pi^+} = 1.00 \pm 0.16 \text{ mb}.$$

The angular distributions for all the particles are shown on Fig. 4. Also shown on Fig. 4 are estimates of the background events. In each case the prediction of charge-conjugation invariance is well satisfied.

These angular distributions suggest that these reactions are the results of peripheral interactions. So we may expect that the events conform to the one-pion-exchange Chew-Low[21] formula

$$\frac{d\sigma^2}{dM^2 d\Delta^2} = \frac{f^2}{2\pi} \frac{1}{p_i^2 m_\pi^2} Mk\sigma(M) \frac{\Delta^2}{(\Delta^2 + m_\pi^2)^2},$$

where m_π is the mass of the pion, σ is the pion-nucleon total cross section, p_i is the laboratory-system momentum of the incident antiproton, Δ^2 is the invariant four-momentum transfer for one nucleon (or antinucleon), M is the effective mass of the other two particles, k is the momentum of either of the other two particles in their own center of mass, and f^2 is the renormalized pion-nucleon coupling constant. This formula predicts that the $\bar{p}p\pi^0$ cross section should be nearly twice as great as the cross section for the other two channels because in this region the cross section is dominated by the (3/2, 3/2) resonance, and for the $T = 3/2$ state the $\pi^0 p$ cross section is twice that of $\pi^+ n$ or $\pi^- p$. Our data give $\frac{2\sigma_{\bar{p}p\pi^0}}{\sigma_{\bar{p}n\pi^+} + \sigma_{p\bar{n}\pi^-}} = 1.69 \pm 0.28$, in agreement with

the peripheral-model prediction, and in disagreement with the prediction of 0.8 given by the statistical model.

Figure 5 shows a scatter diagram of the $\bar{p}p\pi^0$ events in which the coordinates are essentially M^2 and Δ^2. The ordinate has been distorted in such a way that the points in any vertical strip would uniformly populated according to the Chew-Low formula, if σ were constant.[22] This plot illustrates the concentration of events at small values of momentum transfer. The projected distribution on the Δ^2 axis has the features of the prediction of the Chew-Low formula. However, there are many more events at low momentum transfer than predicted by this formula. The Chew-Low formula would be strictly applicable to our experiment only if we knew which pion-nucleon pair was resonating, that is to say with which nucleon to associate the pion. Since we do not know this, the prediction must be modified to include the other pion-nucleon pair. The dotted curve on Fig. 5 is the prediction for the momentum-transfer distribution based on the assumption that (a) the Chew-Low formula gives the correct momentum-transfer distribution for one of the nucleons, that (b) the momentum-transfer distribution of the other nucleon is determined statistically, and that (c) what we observe is the sum of these two distributions. That this curve does not agree with the data indicates that the Δ^2 term in the numerator of the Chew-Low formula is not appropriate. The solid line on Fig. 5 shows the prediction of a peripheral-scattering model in which the Δ^2 dependence is only the propagator $(\Delta^2 + m_\pi^2)^{-2}$, rather than $\Delta^2(\Delta^2 + m_\pi^2)^{-2}$. This curve is a much better fit to the data than are any of the other curves. Such a Δ^2 dependence of the cross section cannot arise from the exchange of a pion in p wave, as is required for $N^*_{3/2}$ production, but could be the correct form if the particle exchanged were a vector meson.

Figure 6 shows histograms of the distributions of the pion-nucleon effective-mass squared for each of the reactions. In every case the data are consistent with charge-conjugation invariance. This is illustrated in Fig. 7, where the distributions of all of the pion-nucleon effective masses are compared with the distributions of the sums of all of the pion-antinucleon effective masses. These two distributions should be identical, according to charge-conjugation invariance. These distributions do not agree well with the phase-space prediction, nor with the predicted distribution corresponding to all the events involving the production of a pion-nucleon or a pion-antinucleon pair in the (3/2, 3/2) resonance. The prediction based on the Chew-Low formula is essentially identical to this latter distribution. The data would fit such a resonance model if the mass of the $N^*_{3/2}$ were assumed to be 1210 MeV rather than 1238 MeV. Perhaps such a shift can effectively be produced by interference between the $N^*_{3/2}$ and the $\overline{N}^*_{3/2}$.

V. ANNIHILATIONS YIELDING ONLY PIONS

There were 1404 events analyzed as annihilations producing pions. From this sample were excluded all events fitting any two-body process (including 14 events fitting two-meson annihilation) with a $\chi^2<30$, and all events fitting any of the three-body inelastic interactions with $\chi^2 < 5$. In this sample there is a contamination of $16 \pm 4\%$ of events that are not pion annihilations: the largest contamination consists of annihilations involving kaons, as can be seen in Table I. We also estimate that $8 \pm 1\%$ of the true pion annihilations have been excluded from this sample. Previous analysis[3] of the annihilations at 1.61 BeV/c indicated that the multiplicities were consistent with the predictions of a statistical model that uses an interaction volume

$\Omega = 5$, where the volume is measured in units of the volume of a sphere having a radius equal to the Compton wavelength of the pion. This model predicts that the sample of two-prong pion annihilations consists of 11% three-body, 36% four-body, 37% five-body, 14% six-body, and 2% seven-body annihilations.

Figure 8a shows the distribution of the square of the missing mass for these events: namely, the square of the effective mass of the neutral particles. Figure 8b shows the same distribution for a sample of simulated events generated by the FAKE program according to the statistical-model prediction. In both cases the solid curve represents the predicted phase-space distribution corresponding to the statistical model with $\Omega = 5$ for all but the three-body events. This model predicts far too many events with missing mass less than 1 BeV, a region populated predominantly by the four-body annihilations. A much better fit to the data is obtained by reducing the predicted number of four-body annihilations by a factor of 1.6 while maintaining the ratio of the other modes the same. This calculation is shown as the dashed curve on Fig. 1a.

The missing-mass distribution shows no compelling evidence for the production of resonances. The π^0 peak is present in the real data with about the same strength as it is in the data from FAKE; this indicates that on the order of 100 $\pi^+\pi^-\pi^0$ events are included in the sample. One might well expect to see evidence for the reaction $\bar{p} + p \rightarrow \pi^+ + \pi^- + \eta$, $\eta \rightarrow$ neutrals, even though no evidence for the η has been seen in other $\bar{p}$ annihilations. By chance, the FAKE data show, if anything, more evidence for η production than do the real data. We estimate that there are 20 ± 20 η's present in these data.

There is no evidence for a peak at the mass of the ρ meson or at the mass of the ω meson. This is not surprising since the ρ is not expected to have an all-neutral decay mode and the all-neutral decay mode of the ω has a small branching ratio.

Figure 9a shows the distribution of the square of the effective mass of everything other than one of the visible pions. In other words, it is the momentum distribution of the charged pions expressed in terms of effective mass. The distributions corresponding to the π^+ and the π^- were in good agreement with each other and were combined. We note that there is no evidence for the reaction $\bar{p}+p \rightarrow \rho^{\pm} + \pi^{\mp}$ for any decay mode of the ρ meson. Figure 9b shows the same distribution for the FAKE data. Just as was the case in Fig. 8, the solid curves represent the statistical-model prediction corresponding to $\Omega = 5$. Again, this curve does not agree well with the data because it is too high in the low effective-mass region dominated by the three- and four-body annihilations. Both phase-space calculations and the FAKE data show that for effective masses less than 1 BeV, the three-body annihilations are dominant. Then, on the assumption that the three-body annihilations are distributed according to a phase-space distribution -- an assumption supported in the next section -- we estimate that there are 122 ± 35 three-pion events in this sample. On the basis of this and the information gained from the missing-mass distribution, we have a new estimate of the composition of these events: 8% three-body, 23% four-body, 48% five-body, 18% six-body, and 3% seven-body. This model is used to calculate the dashed curve on Fig. 9a, as well as the dashed curves on Fig. 8 and Fig. 10. This curve fits the data very well. There is no evidence for substantial production of charged resonances with a single pion.

Figure 10a shows a histogram of the distribution of the effective mass of the $\pi^+\pi^-$ pair, and Fig. 10b is the same distribution for the FAKE events. Again, the dashed curve, which is the phase-space prediction according to the model used to fit the other effective-mass data, is a better fit to the data than is the prediction of the statistical model with $\Omega = 5$ -- although in this case the preference is not as marked as it was in the other cases. Neither of the curves is a good fit to the data. The most striking feature of the data is the overpopulation around 1.3 BeV. However, this peak is no more impressive than is the peak near 1.1 BeV in the FAKE data.

From the study of the four-prong annihilations[10] it is known that considerable numbers of ρ^0 mesons are produced in five-pion annihilations. However, Fig. 10 does not show much evidence for the presence of ρ^0 mesons. If there are about 30 ρ mesons here, as one would estimate from the four-prong data, then both phase-space curves are too high in this region. A lowering of these curves would produce a better fit to the data from 800 MeV to 1 BeV, but would produce a poorer fit to the data near 500 MeV.

Figure 11 is a histogram of the c.m. angular distribution of the π^- and the π^+, as well as the combined distribution obtained by adding the number of events in the $(-\cos\theta_{\pi^+})$ bin to the events in the $(+\cos\theta_{\pi^-})$ bin. None of these distributions is consistent with isotropy. They exhibit an effect similar to that seen in the four-prong annihilations:[5] namely, that there is a peaking in the forward direction for the π^-, and a peaking in the backward direction for the π^+. The question arises as to what extent could this be the effect of misinterpreted events in this sample rather than a property of the pion annihilations. The peaking in the forward direction for the negative particles can be

enhanced somewhat by the $\bar{p}+p \rightarrow \bar{p}+p+\pi^0$ and $\bar{p}+n+\pi^+$ events, and the $\pi^-+p \rightarrow \pi^-+p+\pi^0$ events, since in all these reactions the angular distribution of the negative particle is peaked in the forward direction. However, the number of these events in the sample is not sufficient to produce the effect observed for the negative particles. Furthermore, these events cannot produce the backward peaking of the positive particle observed in Fig. 11. The reason is as follows: In order to obtain the c. m. angle for Fig. 11, the assumption was made that each particle was a pion. If the particle were heavier than a pion, the calculated pion c. m. angle would be too small. Even if there are in the sample protons going predominantly in the backward region (c. m.), they will not produce much of a backward peaking when the mass is assumed to be a pion mass.

The angular distributions of the kaons and pions in annihilations involving kaons deviate very little from isotropy. For the kaons in the sample, misinterpretations of the mass of the particle will produce a small amount of peaking in the forward direction for both the positive and negative curves. Thus the major effect of the misinterpreted events should be to destroy the condition imposed by charge-conjugation invariance that the π^+ and π^- angular distributions should be reflections of each other. A χ^2 test indicates that there is a 10% probability that two distributions from the same sample would disagree as much as do the observed π^+ and π^- angular distributions, whereas there is less than 0.1% probability that an isotropic distribution would appear as anisotropic as do either of these distributions. Therefore, this effect is almost certainly a real property of pion annihilations.

Since all three of the effective-mass distributions are fitted fairly well by one model, it is probably not far from the correct one. However, it is difficult to estimate the accuracy of the determination of the frequency of the

various annihilation modes, both because of the difficulty in estimating the effect of the background events and because of the uncertainty about the assumption, implicit in this analysis, that the phase-space distributions are correct representations of the data.

VII. THREE-PION ANNIHILATIONS

From the foregoing analysis we estimate that there are about 110 events of the reaction $\bar{p} + p \rightarrow \pi^+ + \pi^- + \pi^0$ in the pion-annihilation sample. These events are interesting ones in which to look for two-pion resonances because no other types of resonances can be present. However, it is difficult to get a fairly pure sample of these events to analyze, because the fit to this process is overdetermined by only one constraint, and the average error on missing mass is on the order of a pion mass. The χ^2 distribution (Fig. 12a) for the fits to these three-pion annihilations illustrates the problem. Whereas the χ^2 distribution for the pure events should essentially go to zero when χ^2 is equal to 10, the observed distribution has a long "tail" of events that cannot be real events. That there is a large contamination is further evidenced by the fact that there are 270 events with $\chi^2 < 5$ in this sample -- more than twice as many as we expected to have. A third indication that the background is great is that the distribution of missing-mass squared for those events with $\chi^2 < 5$ (Fig. 13) is strongly weighted to the large-mass side of one-pion mass. Almost all these contamination events are other annihilation events. By observing the two-prong events that have associated kaon decays, we estimate that 20 ± 10 of the events with $\chi^2 < 5$ for three-pion annihilation

are annihilations involving kaons. The rest of the contamination events are four-, five-, and six-body two-prong annihilations that fit the three-body hypothesis.

It is common practice to analyze a χ^2 distribution, such as that on Fig. 12, by observing that the "tail" on the distribution is 10 or 15 events high and by assuming that this amount can be subtracted from the total number of events in the bins at small χ^2 in order to obtain an estimate of the actual number of events that correspond to the hypothesis being tested. In the present case such a method indicates that there are about 200 three-pion annihilations in the sample. That such a method is wrong when one is dealing with a singly constrained (1C) fit is illustrated by the χ^2 distribution for the three-pion assumption obtained by using the FAKE four-pion events (Fig. 12b). The above method would lead to an estimation that there were about 60 three-pion events in a sample composed entirely of four-pion events.

To understand the shape of the χ^2 distribution to be expected when one tries to fit to an hypothesis with one constraint events that are not in agreement with that hypothesis, the following observation is instructive. If one has a set of events for which the distribution in the square of the missing mass is equally populated for all values of missing mass and if the error on this quantity is independent of the value of the quantity, then the χ^2 distribution for any 1C hypotheses will be proportional to $1/\chi$. The distribution will be flat when expressed in terms of χ, the square root of χ^2. For the events that agree with the hypotheses, the distribution in χ should be Gaussian with unit variance. Because of these properties, a distribution in χ is usually more useful than one in χ^2, if one wishes to separate the

background from the true events when one is working with a 1C hypothesis. Figure 14a shows the distribution in χ for the experimental data. Figures 14b and 14c show the estimated background due to many-body pion annihilations obtained from the FAKE events.[23] Figure 14d is the estimated distribution in χ due to kaon annihilations, as estimated from the two prongs with observed associated kaon decays. These background distributions, though not flat, are consistent with linearity; this demonstrates the utility of using a χ distribution for background subtraction. Figure 14e shows the result of subtracting the estimated background from the experimental distribution. This graph demonstrates that the background estimation is fairly accurate because the data after the subtraction are consistent with a normal distribution. The distribution indicates that there are about 120 pion events in the sample.

The FAKE data indicate that $15 \pm 4\%$ of the background events that have $\chi^2 < 5$ have the square of the missing mass less than the square of a pion mass. One-half the real three-pion events should satisfy this criterion. From this, we deduce that 130 ± 25 of the events with $\chi^2 < 5$ are three-pion events. By using a direct subtraction of the estimated background from the observed number of events with $\chi^2 < 5$, we find that there are 111 ± 15 three-pion events with $\chi^2 < 5$.

All these calculations are consistent with one another and in good agreement with the statement that there are 125 ± 15 three-pion events in the sample, and 117 ± 15 of these have $\chi^2 < 5$. Therefore the sample of 270 events with $\chi^2 < 5$ is only about 43% pure.

In an effort to purify this sample, only those events with missing-mass squared within 0.2 $(\text{BeV})^2$ of a pion mass were kept. The resultant sample,

which contains 131 events, will be called the "three-pion sample." From the FAKE data we estimate that there are 37 four-pion annihilations and 3 five-pion annihilations in this sample. We also estimate that there are six kaon annihilations and two events that are inelastic pion interactions. This adds up to 48 ± 7 background events, leaving 83 ± 7 three-pion events. From the FAKE data on three-pion events, we estimate that 65 ± 7% of the three-pion events will be in this sample. This leads to yet another estimate of 128 ± 18 for the number of three-pion events in the pion-annihilation sample. Thus, the data are self-consistent and the three-pion-annihilation sample is 63 ± 5% pure. This sample, impure as it is, is the one used to investigate the three-pion annihilations.

Figure 15 shows an effective-mass-squared scatter diagram for the events in the three-pion sample, and the projections of this distribution for each of the pion pairs is shown on Fig. 16. The distributions are consistent with a phase-space distribution. The FAKE data indicate that the background events produce effective-mass distributions that are fairly consistent with phase-space predictions. These data indicate that at 1.6 BeV/c the three-pion annihilation mode does not often arise from the reaction $\bar{p}+p \rightarrow \rho + \pi$, for there is not a significant surplus of events with an effective mass near 750 MeV. This is in contrast with annihilations at rest, where the ρ is observed to be a prominent constituent of the three-pion annihilations.[24]

The angular distributions (Fig. 17) of the charged pions in these three-pion events are not isotropic. The π^- goes predominantly in the forward direction and the π^+ in the backward direction in the c.m. system, as was observed in the total two-prong sample. The π^+ and π^- angular distributions are consistent with the constraint imposed by charge-conjugation

invariance that they be reflections of each other. When the two distributions are combined, one finds that the ratio of negative pions going forward to those going backward is 1.54 ± 0.19.

VIII. CONCLUSION

The elastic-scattering data show that there is a second diffraction peak at about $\cos\theta = 0.14$. Using these data to determine the scattering amplitudes for each partial wave gives information about the "shape" of the proton when it interacts with an antiproton.

The inelastic events agree with the predictions of charge-conjugation invariance and serve to test this conservation principle. These events are peripheral in nature though they more heavily populate the low-momentum-transfer region than even the one-pion-exchange model predicts.

No resonances are observed in the two-prong annihilation data. Even the ρ meson does not show up significantly in these annihilations.

The cross sections of the various modes of two-prong interactions of 1.61-BeV/c antiprotons in hydrogen have been found to be

$$\bar{p} + p \rightarrow \begin{cases} \bar{p} + p & 31.1 \pm 2 \text{ mb} \\ \bar{p} + p + \pi^0 & 1.85 \pm 0.22 \text{ mb} \\ p + \bar{n} + \pi^- & 1.19 \pm 0.16 \text{ mb} \\ \bar{p} + n + \pi^+ & 1.00 \pm 0.16 \text{ mb} \\ \pi^- + \pi^+ + \pi^0 & 1.58 \pm 0.25 \text{ mb} \\ \text{annihilations}^{8} \text{ with kaons} & 3.4 \pm 0.5 \text{ mb} \\ \pi^+ + \pi^-\ ^{25} & 0.119 \pm 0.030 \text{ mb} \\ K^+ + K^-\ ^{25} & 0.055 \pm 0.018 \text{ mb} \\ \text{other annihilations} & 13.9 \pm 1.5 \text{ mb} \end{cases}$$

We wish to thank Professor Luis Alvarez for his encouragement and support in this experiment. The great help of Dr. Philippe Eberhard in the early stages of the experiment is very gratefully acknowledged.

FOOTNOTES AND REFERENCES

* Work done under the auspices of the U. S. Atomic Energy Commission.

1. J. Button, P. Eberhard, G. R. Kalbfleisch, J. E. Lannutti, G. R. Lynch, B. C. Maglić, and M. L. Stevenson, Phys. Rev. Letters 4, 530 (1960).

2. J. Button, P. Eberhard, G. R. Kalbfleisch, J. E. Lannutti, G. R. Lynch, B. C. Maglić, M. Lynn Stevenson, and N. H. Xuong, Phys. Rev. 121, 1788 (1961).

3. Gerald R. Lynch, Rev. Mod. Phys. 33, 395 (1961).

4. N. H. Xuong, G. R. Lynch, and C. K. Hinrichs, Phys. Rev. 124, 575 (1961).

5. B. C. Maglić, G. R. Kalbfleisch, and M. L. Stevenson, Phys. Rev. Letters 7, 137 (1961).

6. B. C. Maglić, L. W. Alvarez, A. H. Rosenfeld, and M. L. Stevenson, Phys. Rev. Letters 7, 178 (1961).

7. N. H. Xuong and G. R. Lynch, Phys. Rev. Letters 7, 327 (1961).

8. George Kalbfleisch, A Study of K Mesons in Antiproton-Proton Annihilation (Thesis), Lawrence Radiation Laboratory Report UCRL-9597, March 1961 (unpublished).

9. M. L. Stevenson, L. W. Alvarez, B. C. Maglić, and A. H. Rosenfeld, Phys. Rev. 125, 687 (1962).

10. J. Button, G. R. Kalbfleisch, G. R. Lynch, B. C. Maglić, A. H. Rosenfeld, and M. Lynn Stevenson, Phys. Rev. 126, 1858 (1962).

11. C. K. Hinrichs, B. J. Moyer, J. A. Poirier, and P. M. Ogden, Phys. Rev. 127, 617 (1962).

12. N. H. Xuong and G. R. Lynch, Nuovo Cimento 25, 923 (1962).

13. J. Button and B. C. Maglić, Phys. Rev. 127, 1297 (1962).

14. N. H. Xuong and G. R. Lynch, Phys. Rev. 128, 1849 (1962).

15. T. Elioff, L. Agnew, O. Chamberlain, H. Steiner, C. Weigand, and T. Ypsilantis, Phys. Rev. Letters 3, 285 (1959).

16. R. Armenteros, C. H. Coombes, B. Cook, G. R. Lambertson, and W. Wenzel, Phys. Rev. 119, 2068 (1960).

17. Gerald R. Lynch, Program FAKE: Monte Carlo Simulation of Bubble Chamber Events, Lawrence Radiation Laboratory Report UCRL-10335, July 1962.

18. For a description of this δ-ray method, see reference 2.

19. K. R. Greider, and A. E. Glassgold, Ann. Phys. 10, 100 (1960).

20. A. Pais, Phys. Rev. Letters 3, 242 (1959).

21. G. F. Chew and F. E. Low, Phys. Rev. 113, 1640 (1959). Also, F. Bonsignori and F. Selleri, Nuovo Cimento 15, 465 (1960).

22. If the events were populated uniformly in phase space, then the density on this plot would be proportional to M^{-2}.

23. The number of 4π, 5π, and 6π events used to make these estimates corresponds to the statistical-model estimate described in Section VI. This model fitted the data better than did the empirical model that was used to fit the many-pion annihilations.

24. G. B. Chadwick, W. T. Davies, M. Derrick, C. J. B. Hawkins, J. H. Mulvey, D. Radojicic, C. A. Wilkinson, M. Cresti, S. Limentani, and R. Santangelo, in Proceedings of the 1962 International Conference on High-Energy Physics at CERN (CERN, Geneva, 1962), p. 69.

25. G. R. Lynch, P. Eberhard, G. R. Kalbfleisch, J. E. Lannutti, B. C. Maglić, J. B. Shafer, M. L. Stevenson, and N. H. Xuong, Two-Meson Annihilations of 1.61 BeV/c Antiprotons in Hydrogen, Phys. Rev. (to be published). Continuation of ref. 25 accompanying paper UCRL-10633.

Table I. Numbers of events in experimental categories A through E and estimates of the composition of each category. See the text for definitions of categories A through E and groups 1 through 5.

	1	2	3	4	5	Total
A	470 ± 100	108 ± 21	55 ± 11	46 ± 5	232 ± 53	920
B	7^{+10}_{-5}	641 ± 12	0	0	5 ± 5	653
C	9 ± 5	0	293 ± 11	13 ± 4	46 ± 7	361
D	32 ± 20	18 ± 10	26 ± 8	150 ± 38	1190 ± 45	1416
E	32 ± 5	1 ± 1	15 ± 2	117 ± 2	54 ± 7	219
Total	560 ± 100	768 ± 26	399 ± 17	322 ± 40	1527 ± 72	3569

Table II. Values of η_ℓ corresponding to the best fits to the elastic-scattering data. Solutions 1 through 4 are the best 12-parameter solutions obtained. Solution 5 is the 6-parameter solution.

Solution		1	2	3	4	5
	$\ell = 0$	0.182	-0.546	-0.386	-0.181	-0.701
	1	0.017	-0.029	0.042	0.083	0.027
$\mathrm{Re}(\eta_\ell)$	2	0.183	0.330	0.317	0.261	0.316
	3	0.419	0.531	0.530	0.509	0.543
	4	0.676	0.679	0.663	0.688	0.672
	5	0.866	0.813	0.809	0.838	0.840
	0	0.185	0.165	0.727	-0.277	0
	1	-0.165	-0.151	0.343	-0.113	0
$\pm\mathrm{Im}(\eta_\ell)$	2	-0.127	-0.136	0.117	0.201	0
	3	0.037	-0.105	0.119	0.095	0
	4	0.140	-0.072	0.035	-0.024	0
	5	0.130	-0.038	0.039	0.014	0

Table III. Estimates of the composition of the samples of events analyzed as inelastic scatterings.

	True $\bar{p}p\pi^0$ events	True $p\bar{n}\pi^-$ events	True $\bar{p}n\pi^+$ events	Interaction of pions	Annihilation producing only pions	Annihilation producing only kaons	Total
Events in $\bar{p}p\pi^0$ sample	123 ± 5	1 ± 1	3 ± 2	2 ± 2	7 ± 3	1 ± 2	137
Events in $p\bar{n}\pi^-$ sample	1 ± 1	80 ± 6	1 ± 2	2 ± 2	18 ± 4	6 ± 2	108
Events in $\bar{p}n\pi^+$ sample	4 ± 3	1 ± 2	65 ± 7	4 ± 3	18 ± 4	6 ± 2	98
Events eliminated by χ^2 cutoff	12 ± 6	8 ± 4	6 ± 3	—	—	—	
Unanalyzable events	7 ± 1	4 ± 1	4 ± 1	—	—	—	
Total	147 ± 8	94 ± 8	79 ± 9				

FIGURE LEGENDS

Fig. 1. A histogram of the measured differential cross section for elastic scattering of 1.61-BeV/c antiprotons for $\cos\theta < 0.8$. The errors are statistical only. In addition, there is about a 6% systematic uncertainty. The curve corresponds to solution 2 in Table II.

Fig. 2. The differential cross section for elastic scattering of antiprotons of 1.61 BeV/c. The data for $\cos\theta > 0.8$ are previously measured cross-section values, and the data for $\cos\theta < 0.8$ are the data from this experiment. The curves represent the best optical-model fit (dotted curve), the 6-parameter solution (dashed curve), and the best 12-parameter solution (solid curve).

Fig. 3. A plot of the opacity $(1 - |\eta_\ell|^2)$ of the proton-antiproton system for various cases. The smooth curve represents the best four-parameter optical-model fit to the data. The points represent the indicated solutions.

Fig. 4. The angular distributions of the nucleons and antinucleons in the inelastic-scattering events. Figures (a), (b), and (c) are for the $\bar{p}p\pi^0$ reaction, and the others are for the $\bar{p}n\pi^+$ and $p\bar{n}\pi^-$ reactions. Figures (c), (f), and (i) are the appropriate sums of the two figures to the left of each. For each graph, estimates of the background events have been made; the data are plotted in such a way that the background events are plotted negatively; and the remaining events, which are the estimated number of genuine events, are plotted positively.

Fig. 5. A scatter diagram in the M^2, Δ^2 plane, where Δ^2 is the invariant four-momentum transfer of the nucleon or antinucleon and M is the effective mass of the other two particles. The M^2 scale has been distorted in such a way that, according to the Chew-Low formula, any vertical strip would be populated according to $\sigma(M)$, the πp cross section. Each event has been plotted twice on this diagram. A histogram of the projection of these data on the Δ^2 axis is compared with a phase-space prediction (dashed curve); with the prediction indicated by the Chew-Low formula (dot-dash curve); with a modified prediction, based on the Chew-Low formula, including the distribution for both of the nucleons (dotted line); and with a similar prediction based on a peripheral model with a $(\Delta^2 + m_\pi^2)^{-2}$ dependence (solid line). All curves are normalized to the data.

Fig. 6. Histograms of the distributions of the pion-nucleon effective-mass squared for (a) the $p\pi^0$ and $\bar{p}\pi^0$ in the $\bar{p}p\pi^0$ reaction, (b) the $\bar{p}\pi^+$ and $p\pi^-$, and (c) the $\bar{n}\pi^-$ and $n\pi^+$ in the other two reactions. The data are compared with a phase-space estimate (dashed curve), and with the prediction based on the production of either the pion-nucleon pair or the pion-antinucleon pair in the (3/2 - 3/2) resonance (solid curve). All curves are normalized to the data.

Fig. 7. Histograms of the distribution of the effective-mass squared for (a) all the pion-nucleon pairs, and (b) all the pion-antinucleon pairs. The solid curve is the same resonance-model prediction shown in Fig. 6.

Fig. 8. A histogram of the distribution of the square of the missing mass calculated for (a) the real events in the pion-annihilation sample and or (b) the FAKE events. The solid curve is the prediction based on a statistical model with $\Omega = 5$. The dashed curve represents an empirical model discussed in the text.

Fig. 9. A combined histogram of the square of the effective mass of everything except one of the charged particles for (a) the real events in the pion-annihilation sample and (b) the FAKE events. The solid and dashed curves are predictions of the same statistical model and empirical model used in Fig. 8.

Fig. 10. A histogram of the distribution of the effective mass for the $\pi^+\pi^-$ pair for (a) the events in the pion-annihilation sample and (b) the FAKE events. The solid and dashed curves are predictions of the same statistical model and empirical model used in Fig. 8 and Fig. 9.

Fig. 11. A histogram of the c. m. angular distribution of (a) the negative pion, (b) the positive pion, and (c) both pions for the events in the pion-annihilation sample.

Fig. 12. Histograms of the χ^2 distributions for the $\pi^+\pi^-\pi^0$ interpretation for (a) the real events and (b) a sample of 424 simulated four-pion annihilations.

Fig. 13. Histogram of the square of the missing mass for those events in the pion-annihilation sample having $\chi^2 < 5$ for the three-pion interpretation.

Fig. 14. Histograms of the distributions in χ (the square root of χ^2) for (a) the real events, (b) the estimated background from four-pion annihilations, (c) the estimated background from five- and six-pion annihilations, (d) the estimated background from annihilations with kaons, and (e) the difference between the real data and the estimated background.

Fig. 15. An effective-mass-squared scatter diagram for the 131 events in the three-pion annihilation sample. The narrow bands indicate the position of the charged ρ meson. The neutral ρ would show up in a band near the upper right-hand edge of the envelope. However, this band is spread out considerably owing to the spread in the beam momenta. The envelope corresponds to the kinematic limit for 1.61-BeV/c antiprotons.

Fig. 16. A histogram of the distribution in effective-mass squared of (a) the $\pi^+\pi^-$ pair, (b) the $\pi^-\pi^0$ pair, and (c) the $\pi^+\pi^0$ pair for the events in the three-pion sample. The curves are the phase-space predictions normalized to the data.

Fig. 17. Histograms of the c.m. angular distribution for the pions in the three-pion annihilation sample. The π^0 distribution has been folded around 90°.

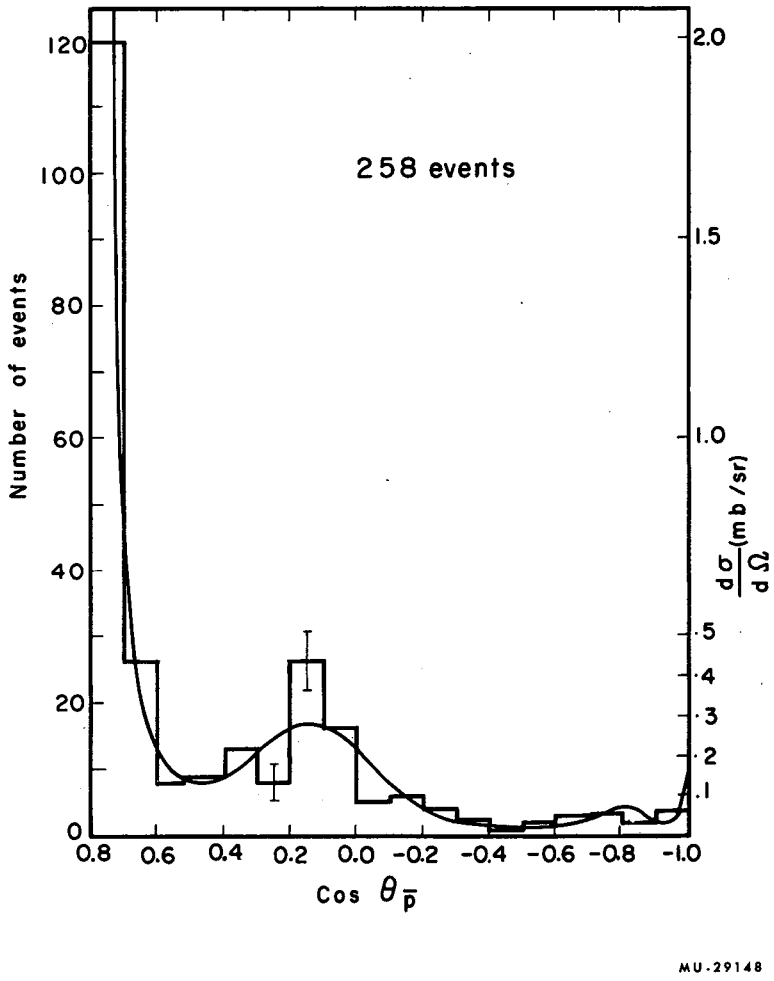
258 events
Number of events
$\frac{d\sigma}{d\Omega}$ (mb/sr)
Cos $\theta_{\bar{p}}$
120
100
80
60
40
20
0
2.0
1.5
1.0
.5
.4
.3
.2
.1
0.8
0.6
0.4
0.2
0.0
-0.2
-0.4
-0.6
-0.8
-1.0
MU-29148

Fig. 1.

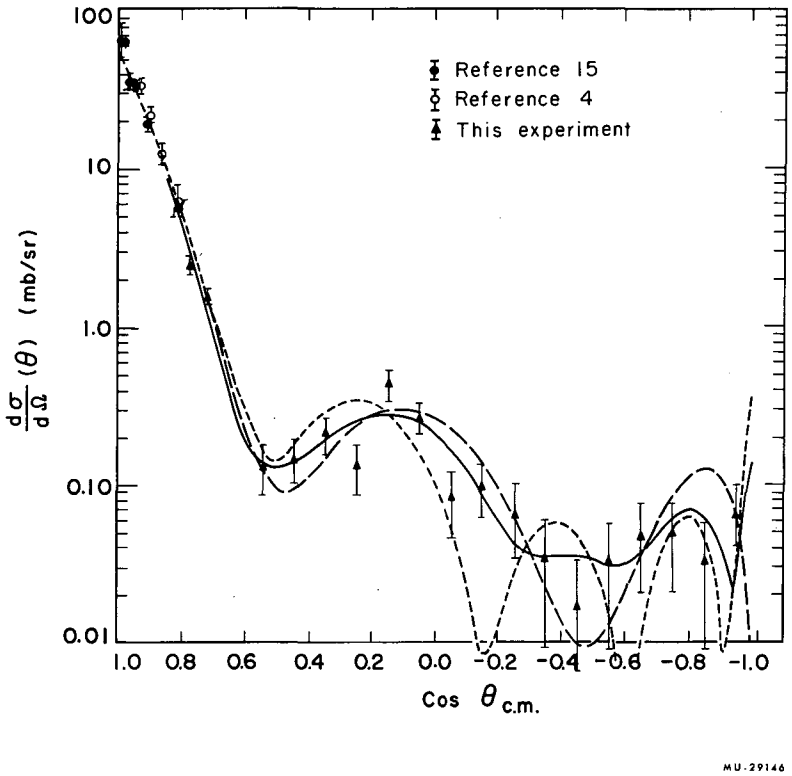
Reference 15
Reference 4
This experiment
100
10
1.0
0.10
0.01
$\frac{d\sigma}{d\Omega}(\theta)$ (mb/sr)
1.0 0.8 0.6 0.4 0.2 0.0 -0.2 -0.4 -0.6 -0.8 -1.0
Cos $\theta_{c.m.}$
MU-29146

Fig. 2.

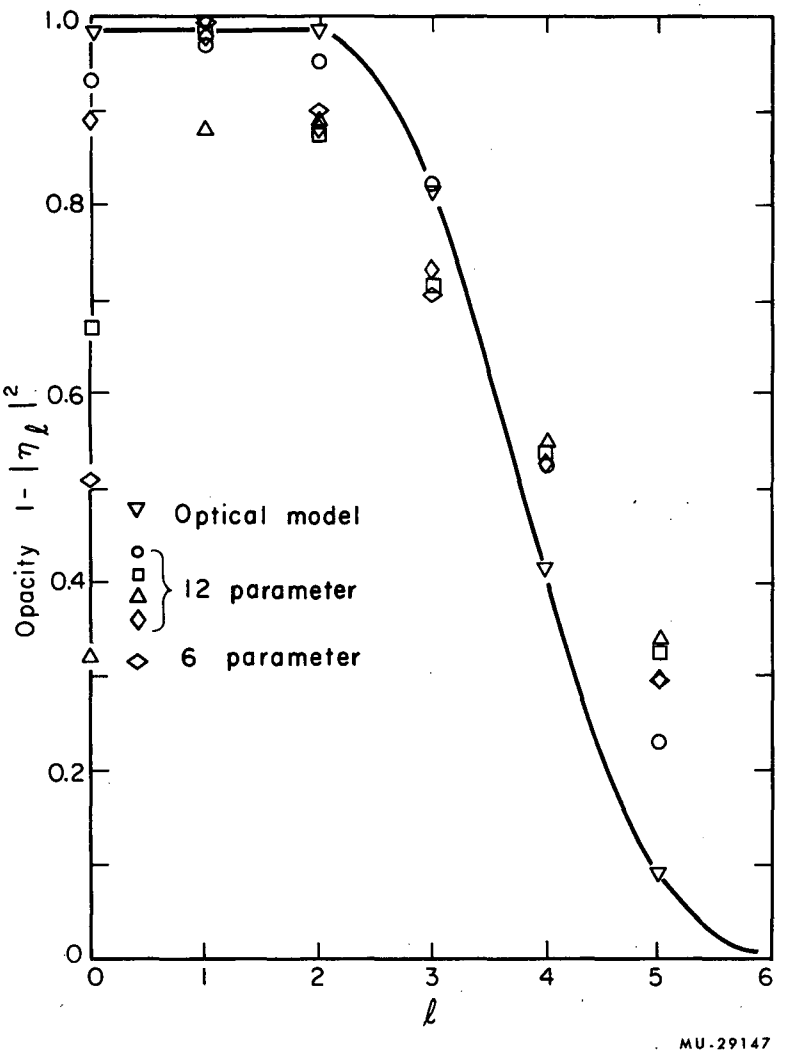
1.0
0.8
0.6
0.4
0.2
0
Opacity $1-|\eta_\ell|^2$
Optical model
12 parameter
6 parameter
0
1
2
3
4
5
6
ℓ
MU-29147

Fig. 3.

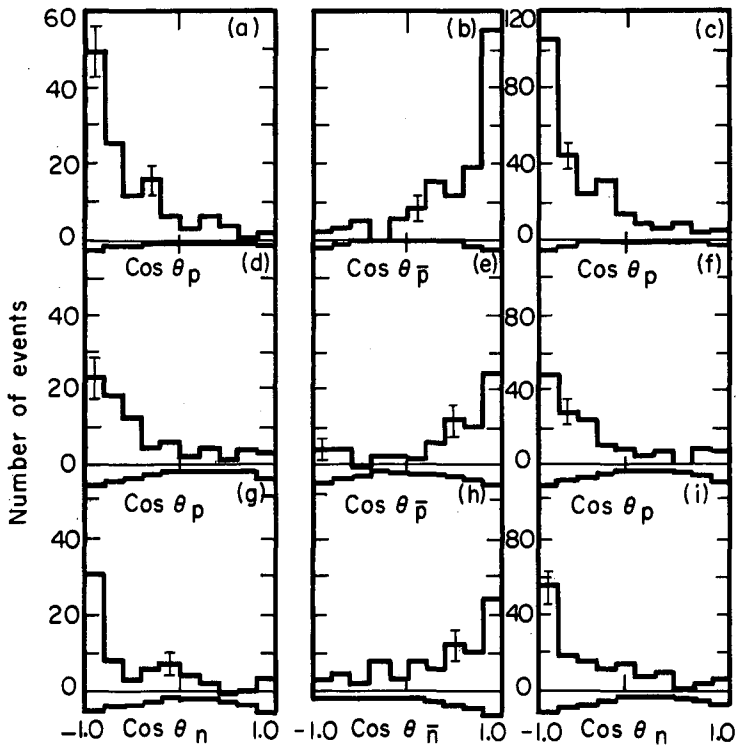
Number of events
(a)
(b)
(c)
(d)
(e)
(f)
(g)
(h)
(i)
Cos θ p
Cos θ p̄
Cos θ p
Cos θ p
Cos θ p̄
Cos θ p
Cos θ n
Cos θ n̄
Cos θ n
-1.0
1.0
MU-29154

Fig. 4.

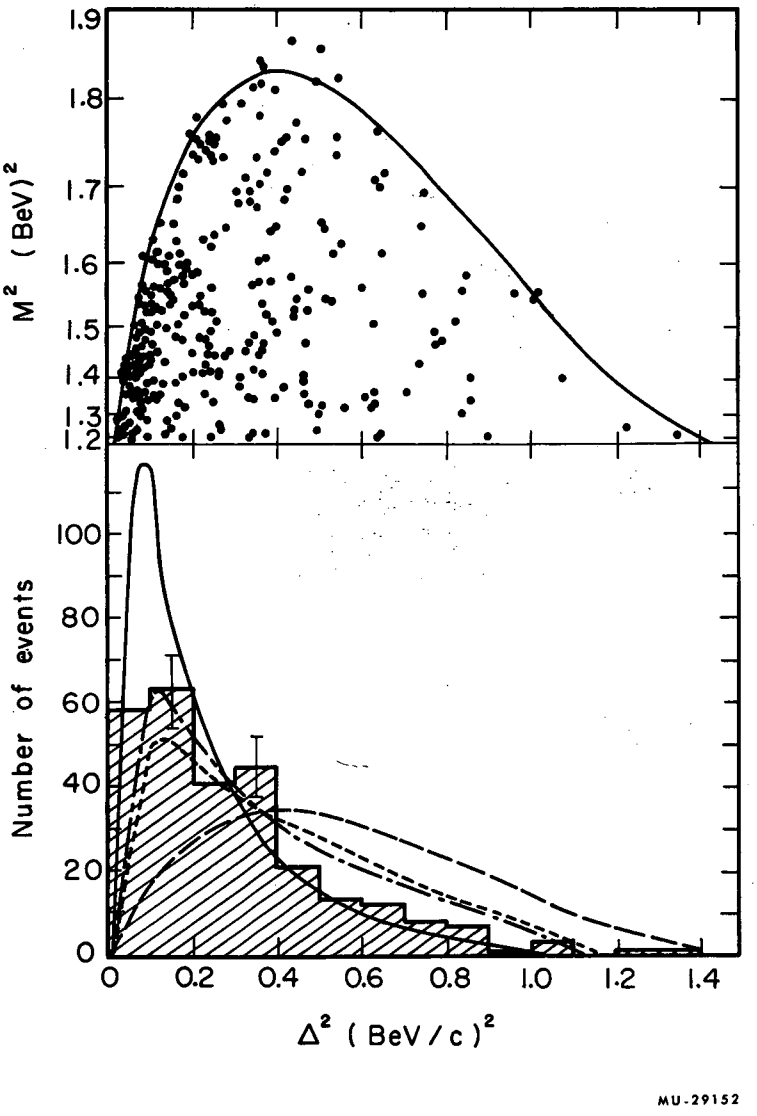
1.9
1.8
1.7
1.6
1.5
1.4
1.3
1.2
M^2 (BeV)^2
100
80
60
40
20
0
Number of events
0
0.2
0.4
0.6
0.8
1.0
1.2
1.4
Δ^2 (BeV/c)^2
MU-29152

Fig. 5.

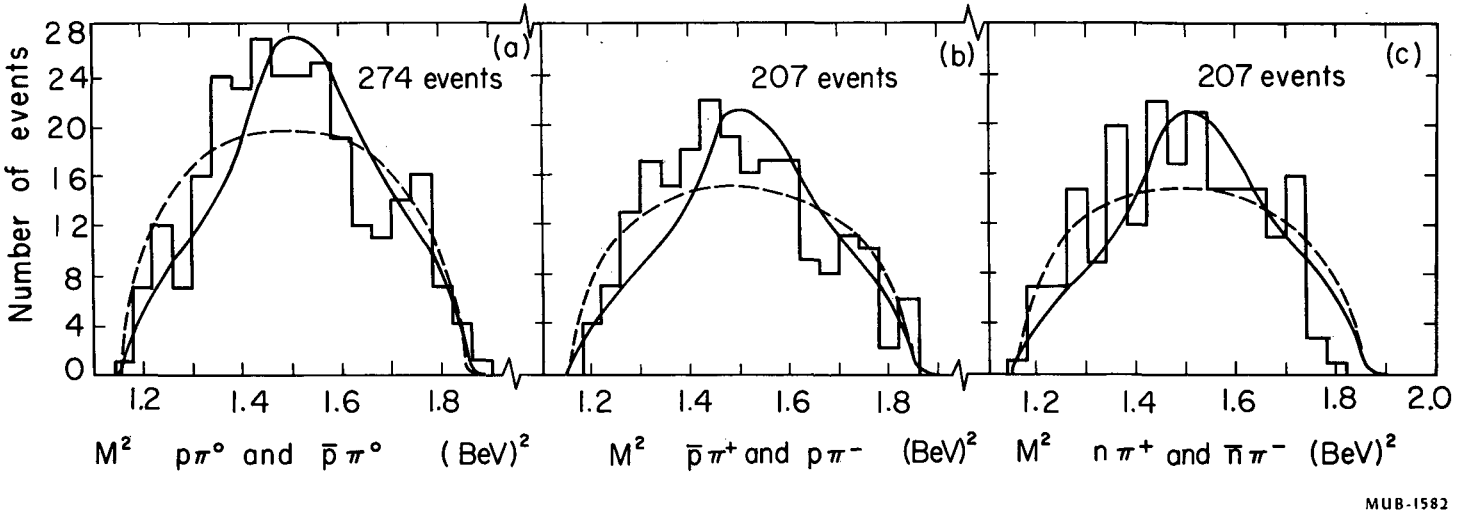
Number of events
28
24
20
16
12
8
4
0
(a)
274 events
(b)
207 events
(c)
207 events
1.2
1.4
1.6
1.8
2.0
M² pπ° and p̄π° (BeV)²
M² p̄π⁺ and pπ⁻ (BeV)²
M² nπ⁺ and n̄π⁻ (BeV)²
MUB-1582

Fig. 6.

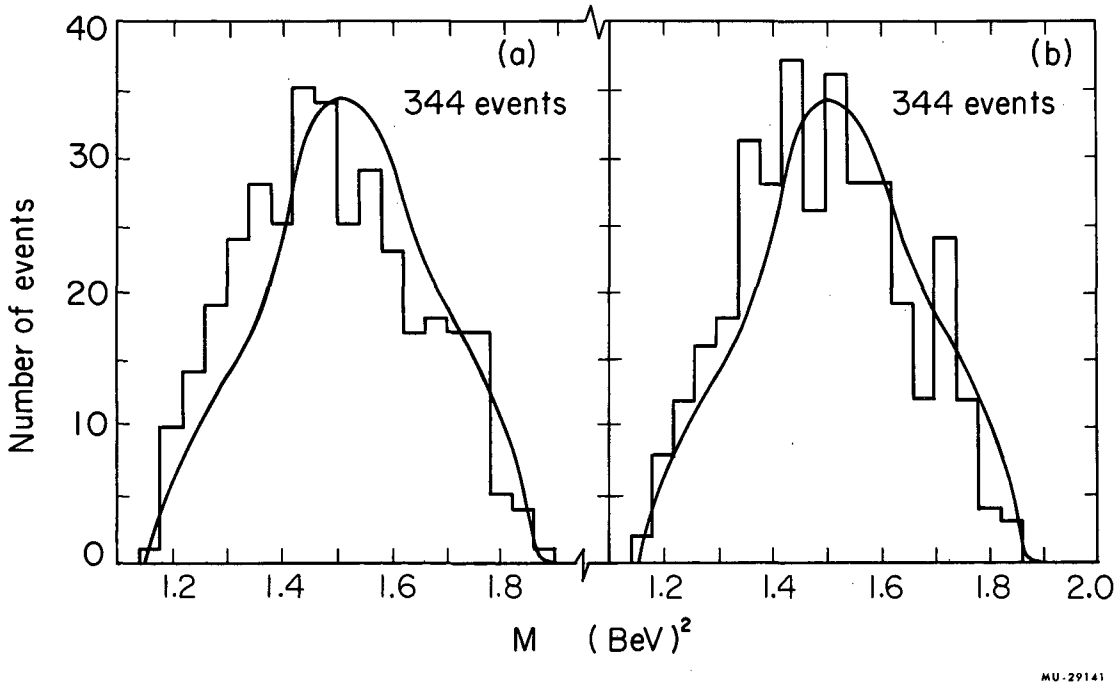
40
30
20
10
0
Number of events
(a)
344 events
(b)
344 events
1.2
1.4
1.6
1.8
2.0
M (BeV)²
MU-29141

Fig. 7.

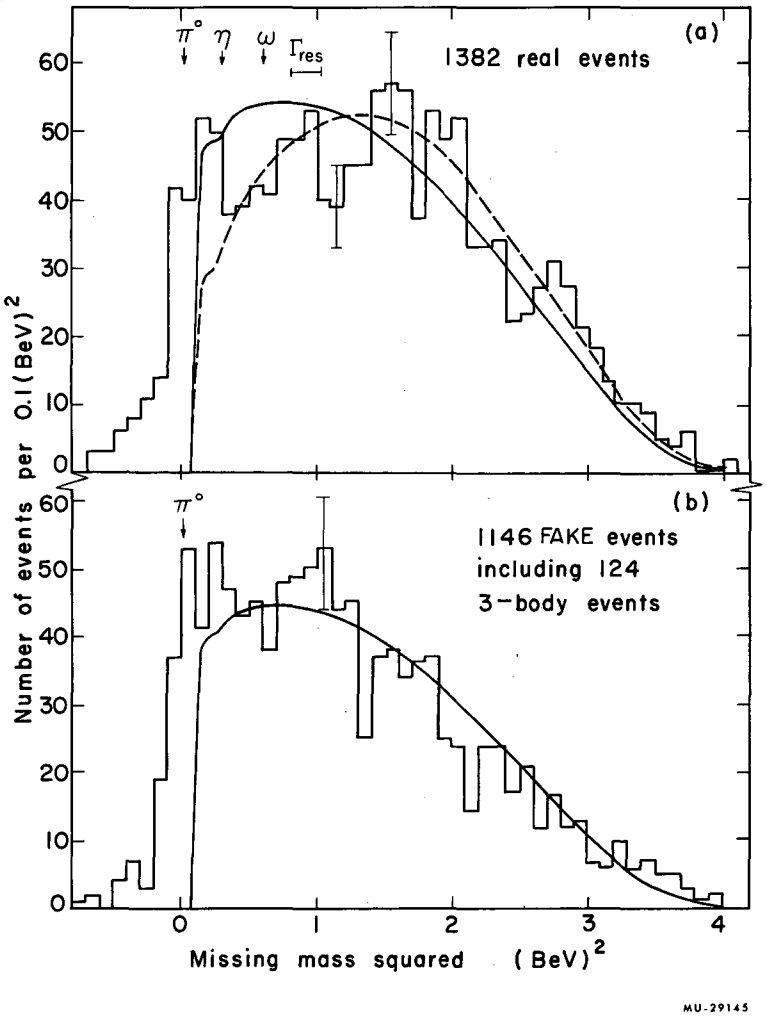
π° η ω Γres
(a)
1382 real events
(b)
π°
1146 FAKE events
including 124
3-body events
Number of events per 0.1 (BeV)²
Missing mass squared (BeV)²
MU-29145

Fig. 8.

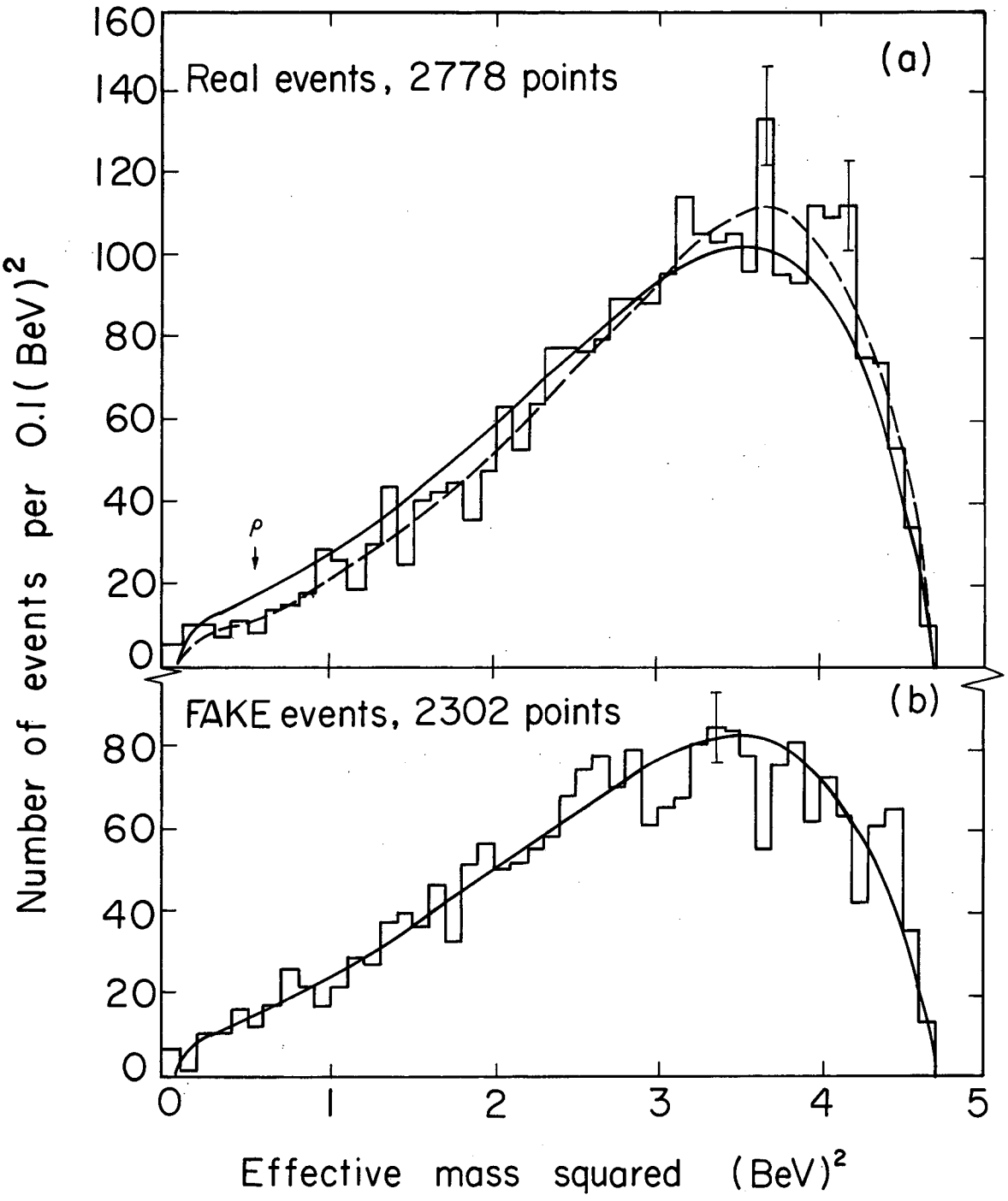
Real events, 2778 points
(a)
ρ
FAKE events, 2302 points
(b)
Number of events per 0.1 (BeV)²
Effective mass squared (BeV)²
0
20
40
60
80
100
120
140
160
0
1
2
3
4
5
MUB-1583

Fig. 9.

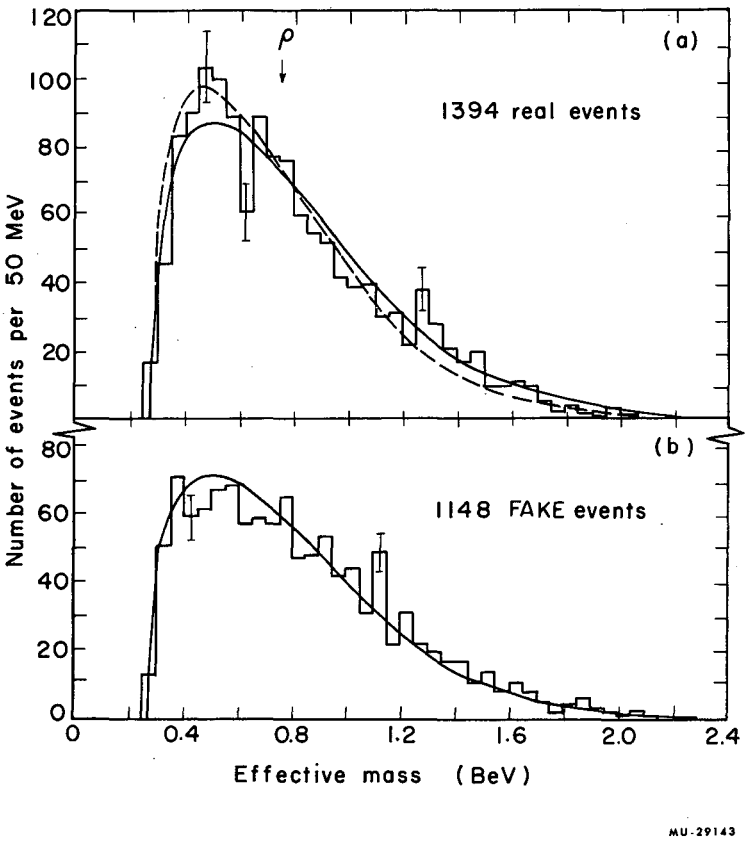
120
100
80
60
40
20
ρ
(a)
1394 real events
(b)
1148 FAKE events
Number of events per 50 MeV
0
0.4
0.8
1.2
1.6
2.0
2.4
Effective mass (BeV)
MU-29143

Fig. 10.

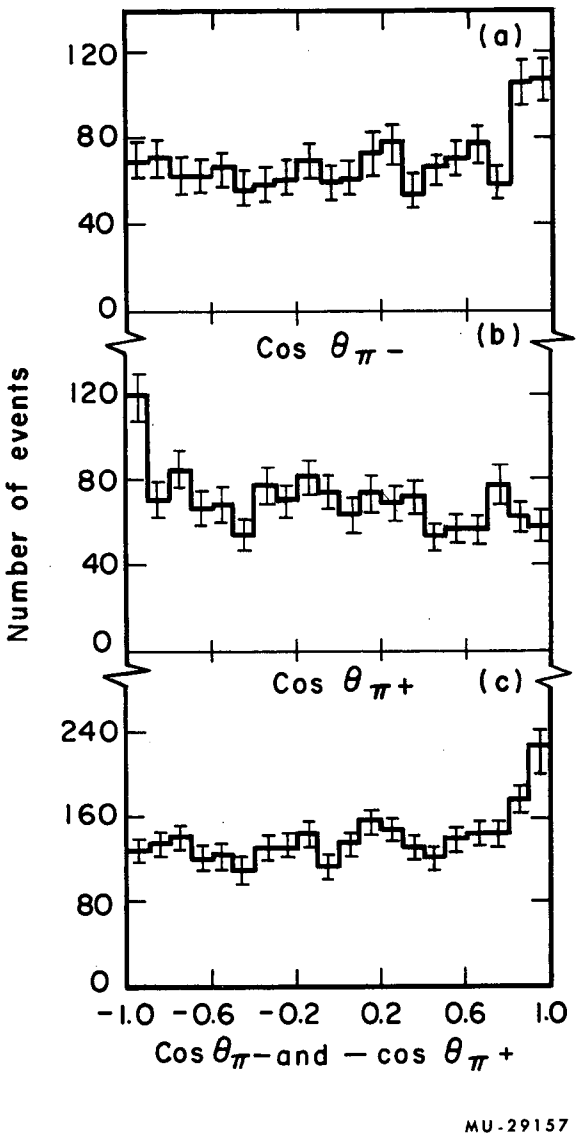
(a)
120
80
40
0
Cos θ_{π^-}
(b)
120
80
40
0
Number of events
Cos θ_{π^+}
(c)
240
160
80
0
-1.0 -0.6 -0.2 0.2 0.6 1.0
Cos θ_{π^-} and $-\cos\theta_{\pi^+}$
MU-29157

Fig. 11.

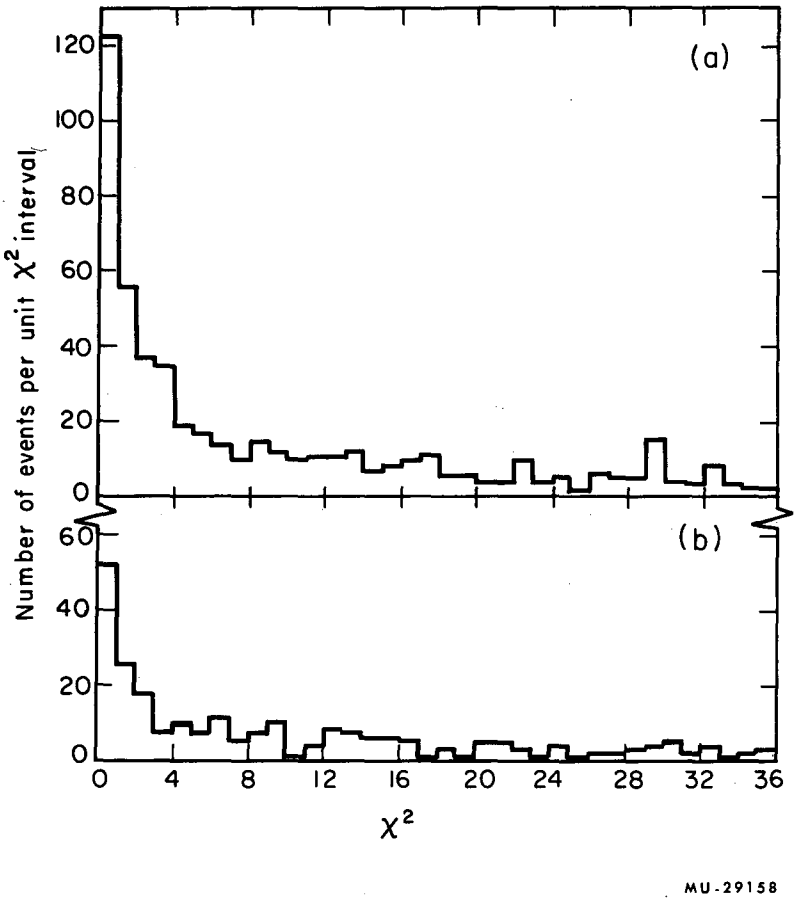
(a)
(b)
Number of events per unit χ^2 interval
120
100
80
60
40
20
0
60
40
20
0
0
4
8
12
16
20
24
28
32
36
χ^2
MU-29158

Fig. 12.

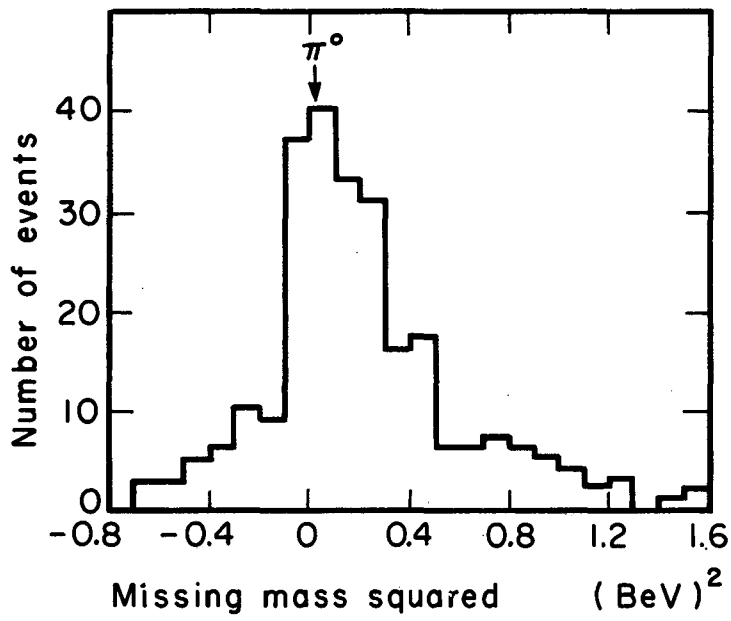

MU-29150

Fig. 13.

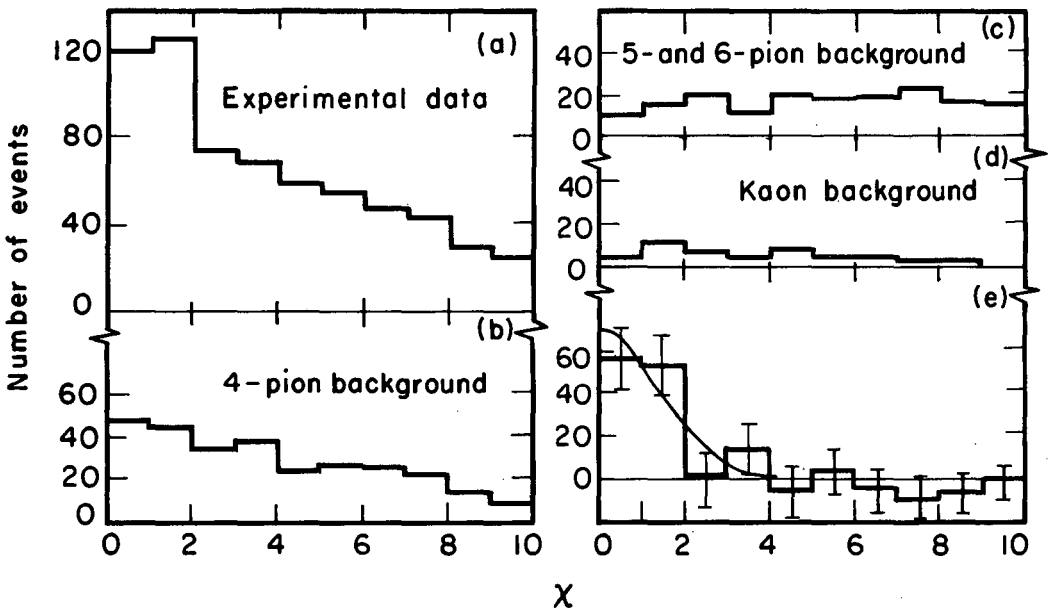
(a)
Experimental data
(b)
4-pion background
(c)
5-and 6-pion background
(d)
Kaon background
(e)
Number of events
χ
MU-29149

Fig. 14.

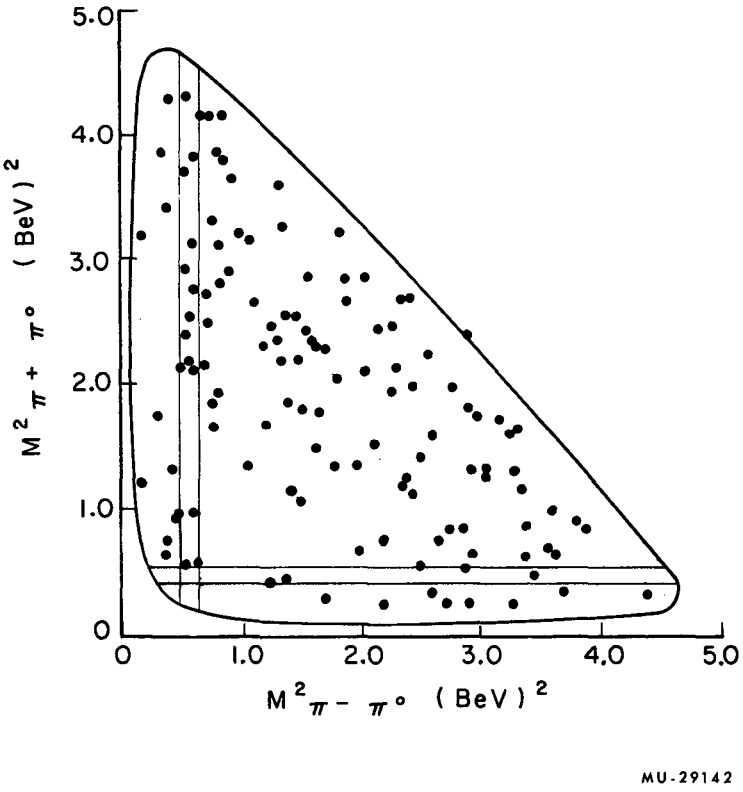
5.0
4.0
3.0
2.0
1.0
0
0
1.0
2.0
3.0
4.0
5.0
$M^2_{\pi^+ \pi^\circ}$ (BeV)^2
$M^2_{\pi^- \pi^\circ}$ (BeV)^2
MU-29142

Fig. 15.

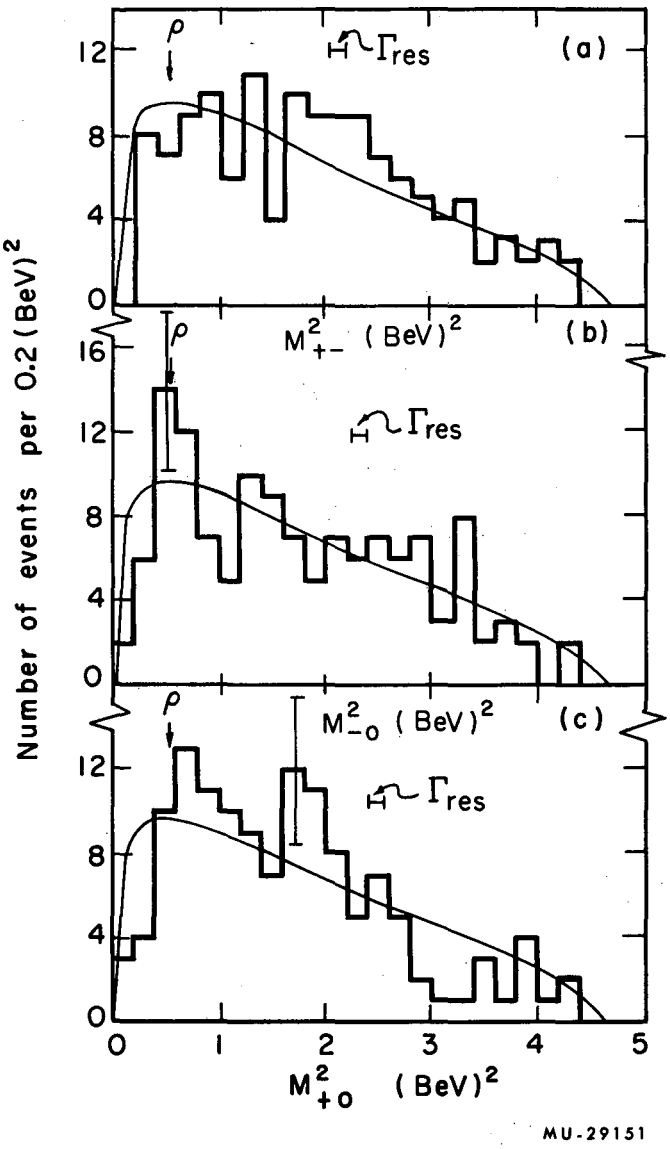
Number of events per 0.2 (BeV)^2
ρ
Γ_{res}
(a)
M^2_{+-} (BeV)^2
(b)
M^2_{-o} (BeV)^2
(c)
M^2_{+o} (BeV)^2
MU-29151

Fig. 16.

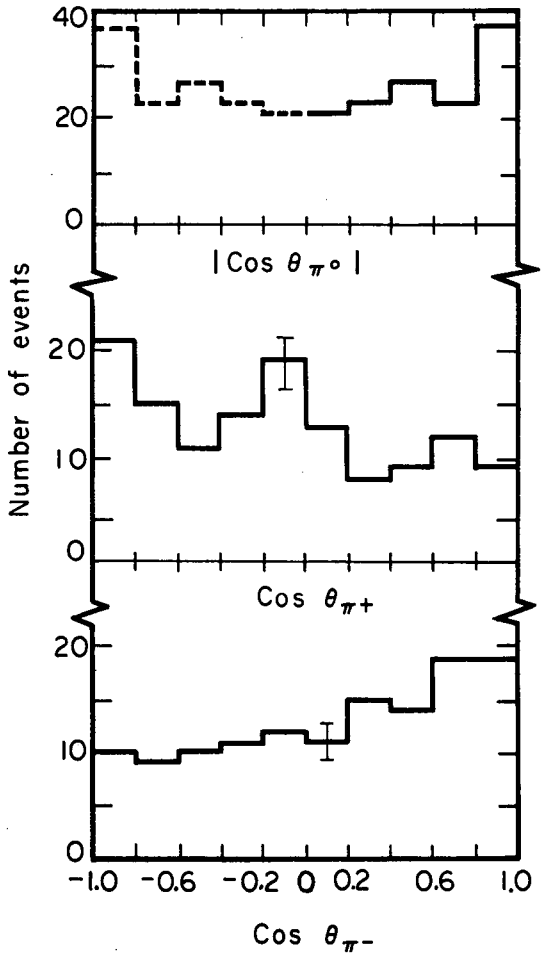
40
20
0
|Cos θπ°|
20
10
0
Number of events
Cos θπ+
20
10
0
-1.0 -0.6 -0.2 0 0.2 0.6 1.0
Cos θπ-
MU-29153

Fig. 17.